

NV⁻ Diamond Laser

Alexander Savvin¹, Alexander Dormidonov¹, Evgeniya Smetanina¹, Vladimir Mitrokhin¹,
Evgeniy Lipatov^{2,3}, Dmitriy Genin^{2,3}, Sergey Potanin^{4,5}, Alexander Yelisseyev⁶, Viktor Vins⁷

 dormidonov@gmail.com

¹Dukhov Automatics Research Institute, Sushchevskaya 22, Moscow 127055, Russian Federation

²National Research Tomsk State University, 36 Lenin ave., Tomsk, 634050, Russian Federation

³Institute of High Current Electronics SB RAS, 2/3 Akademicheskii ave., Tomsk, 634055, Russian Federation

⁴Faculty of Physics, Lomonosov Moscow State University, Leninskie Gory 1, Moscow, 119991, Russian Federation

⁵Sternberg Astronomical Institute, Lomonosov Moscow State University, Universitetskii ave. 13, Moscow, 119234, Russian Federation

⁶V.S. Sobolev Institute of Geology and Mineralogy SB RAS, 3 Koptyug ave., Novosibirsk, 630090, Russian Federation

⁷LLC VELMAN 43, Russkaya str., Novosibirsk, 630058, Russian Federation

Abstract

For the first time, lasing at NV⁻ centers in an optically pumped diamond sample is achieved. A nanosecond train of 150-ps 532-nm laser pulses was used to pump the sample. The lasing pulses have central wavelength at 720 nm with a spectrum width of 20 nm, 1-ns duration and total energy around 10 nJ. In a pump-probe scheme, we investigate lasing conditions and gain saturation due to NV⁻ ionization and NV⁰ concentration growth under high-power laser pulse pumping of diamond crystal.

Introduction

Color centers in diamond exhibit outstanding spectroscopic properties¹ with photoluminescence spectra covering visible and near-IR wavelength ranges²⁻⁶. Optical

transparency of diamond and its excellent mechanical, thermal, and optical characteristics make it a promising host material for color-center photon source^{7, 8}. One of the most studied color centers in diamond, the negatively charged nitrogen-vacancy (NV^-) center, is a unique solid-state quantum system exhibiting high quantum efficiency at room temperature. It can be coupled to dielectric cavities and plasmonic resonators in order to create single-photon emitters applicable in quantum photonic technologies⁹⁻¹¹. Laser initialization, changing and reading the spin state of an NV^- electron allows to control the state of a quantum system and turn NV^- centers in diamond into a promising platform for optical quantum computing¹²⁻¹⁹, quantum metrology, sensing and visualization²⁰⁻²⁵.

For decades, diamond crystals with nitrogen-vacancy centers have been considered as a potential lasing medium^{2, 26, 27}. Nitrogen vacancy color centers exist in two states: negatively charged — NV^- (with its zero-phonon line at 637 nm) and neutral — NV^0 (with its zero-phonon line at 575 nm)¹. Both states support strong electron–phonon interactions that result in a very broad phonon sideband (PSB) emission^{1, 11}. Exhibiting large emission and absorption cross sections, high quantum efficiency and a broad gain band, diamond with NV centers can be considered as a promising solid state active media for tunable and femtosecond lasers in the red and near infrared spectral regions²⁸.

Monocrystalline samples of IIa-type diamond with NV color centers created by means of high pressure and high temperature synthesis (HPHT) are currently available on the market²⁸⁻³⁰. Spectroscopic characteristics of NV^- centers in diamond were investigated in²⁶; however, stimulated emission or lasing at NV centers in diamond have not been achieved in that work. Stimulated emission of NV^- centers in diamond was claimed to be observed in recent work²⁷. A rise of stimulated emission at wavelengths in the PSB of NV^- zero-phonon line (ZPL) was detected by measuring a decrease of the NV^- spontaneous emission under a CW optical pump at 532 nm. However the results presented in²⁷ were based on indirect measurements. Direct

measurements of the optical gain and lasing at NV^- centers in diamond have not been delivered yet.

In this work, we investigated in detail spectral properties of the HPHT diamond sample with two growth zones exhibiting different NV^0 to NV^- concentration ratios. Sample photoluminescence was enhanced by CW and pulsed lasers at various wavelengths. A direct pump-probe method was used for registration of stimulated emission from the diamond sample. We demonstrate that the diamond sample zone with a predominance of NV^0 centers exhibits only pump-induced absorption of the probe, while the growth zone with a high concentration of NV^- centers provides the probe amplification. However, we detect a saturation of the probe amplification and probe absorption that appears due to NV^- ionization and NV^0 formation at sufficiently high pump rates. The maximal detected gain coefficient is about 1.4 cm^{-1} that allows us to reach lasing conditions in the diamond sample zone with a predominant NV^- concentration and, for the first time, we achieve a laser generation at NV^- color centers in diamond.

Results

Spectroscopic characterization of the diamond sample.

An investigated diamond sample is a $4 \times 3 \times 0.25$ mm plate containing two growth zones (Fig. 1) with significantly different NV^0 to NV^- concentration ratios. The largest part of the sample (zone S1) mostly contains neutral NV^0 centers. In a narrow (about $250 \text{ }\mu\text{m}$) dark-colored region at the edge of the sample (zone S2) the concentration of NV^- centers turned out to be significantly higher than the NV^0 concentration. Two lateral faces of the sample were polished at the Brewster's angle (See Methods for more details).

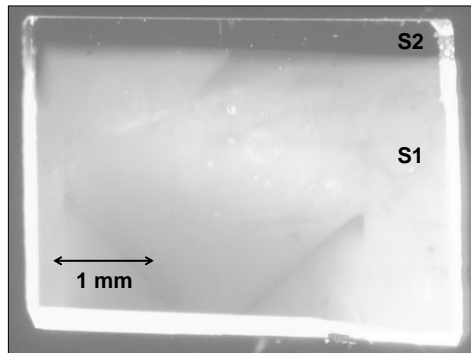


Figure 1 | The diamond sample. Photography of the diamond sample that has two growth zones with significantly different ratios of NV^0 concentration to NV^- concentration. Zone S1 mainly contains neutral NV^0 centers and NV^- concentration dominates in zone S2.

The absorption spectra of the S1 and S2 zones were obtained by illuminating the sample with a tungsten incandescent lamp and are given on Fig. 2a after Fresnel correction in a logarithmic scale (gray and black curves, respectively). The spectra were recorded at room temperature employing an Ocean Optics FLAME-S-XR1 spectrometer with a 200- μm fiber input for sample-transmitted light collection. The obtained optical absorption spectrum of the sample is typical for type IIa diamonds^{1,6}.

The S1-zone absorption spectrum has a maximum at 575 nm and a width of about 150 nm (Fig. 2a, gray curve), which corresponds to the characteristic absorption spectrum of NV^0 centers in diamond^{26,27}. The S2-zone absorption spectrum contains a pronounced absorption band from 500 to 660 nm with a maximum around 569 nm due to the domination of NV^- centers in this zone (Fig. 2a, black curve). At the peak NV^- absorption wavelength, the absorption coefficient reaches 14 cm^{-1} , which is an order of magnitude less than the NV^- -containing diamond sample absorption coefficient measured in²⁶. We observe strong blue absorption in the spectral range from 400 to 495 nm (Fig. 2a, black curve) that indicates a significant amount of nitrogen atoms in the S2 zone³¹. Electrons of nitrogen donor atoms (C-centers) are captured by NV^0 centers, thereby changing their state to NV^- ³². Thus, the presence

of nitrogen atoms in the S2 zone naturally leads to an increase in the NV⁻ concentration and, we believe, is the key difference between the zones S1 and S2.

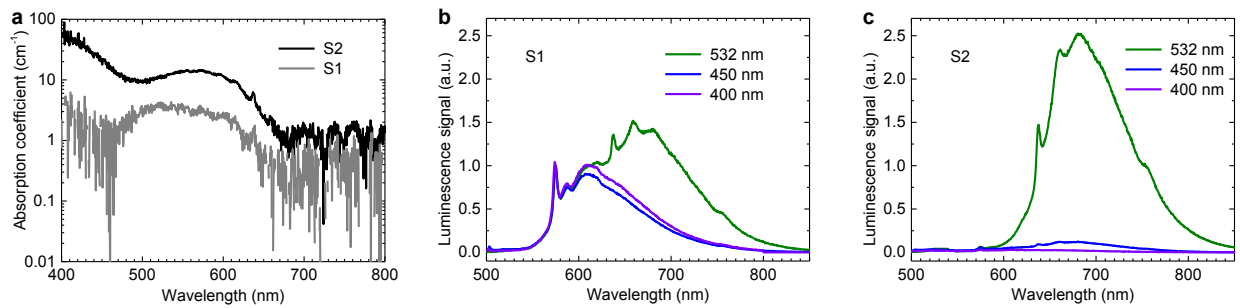


Figure 2 | Spectroscopic characterization of the diamond sample. (a) Absorption spectrum of S1 (gray curve) and S2 (black curve) zones of diamond sample. The spectra were recorded at room temperature. Normalized photoluminescence spectra of S1 **(b)** and S2 **(c)** zones under continuous excitation at various wavelengths: 532 nm (green curve), 450 nm (blue curve), and 400 nm (violet curve). For each pump wavelength the spectra collected from both zones were normalized on the S1-zone spectral amplitude at 575 nm that corresponds to the NV⁰ zero-phonon line. The photoluminescence spectra were collected from the sample excitation surface, i.e. the pump lasers and the recording spectrometer were located on the same side of the sample.

We used three CW lasers with a power of about 10 mW at wavelengths of 400, 450, and 532 nm to illuminate the sample. The sample was mounted on a vertical translation stage with a micrometric step resolution allowing to operate with sample zones S1 and S2 without any readjustment of the experimental set-up. The photoluminescence spectra were collected from the illuminated sample surface, i.e. the incident laser beam and the recording spectrometer were located on the same side of the sample. Normalized photoluminescence spectra of S1 and S2 zones are given in Fig. 2c and d, respectively. For each excitation wavelength, the spectra collected from both zones were normalized on the S1-zone spectral amplitude at 575 nm that corresponds to the NV⁰ ZPL in diamond. The photoluminescence spectra of the zone S1 exhibit a strong NV⁰ centers ZPL at 575 nm and its PSB emission with a maximum at 609 nm at all considered excitation wavelengths (Fig. 2b). ZPL of NV⁻ centers at 638 nm and its PSB emission with a maximum at 680 nm are presented in the photoluminescence spectra of both zones under 532-nm excitation (Fig. 2b,c green curves). The photoluminescence spectra under 400-

and 450-nm excitation for zone S1 are identical (Fig. 2b blue and violet curves) and have much higher amplitudes than the photoluminescence spectra from S2 zone (Fig. 2c blue and purple curves) because both excitation wavelengths fall in the NV⁰ absorption region and are not absorbed by the NV⁻ centers.

The decay time of the spontaneous emission signal integrated over in the wavelength range 670–680 nm was found to be $\tau_{21}=9.3\pm0.3$ ns for the S2 zone with a predominant concentration of NV⁻ color centers. We employed a fast optoelectronic converter to measure τ_{21} (See Methods for more details). The obtained decay time is close to the NV⁻ excited state lifetime given in a number of other works: 8 ± 1 ns in ³³, 7.8 or 12 ns depending on the spin state of the diamond defect ³⁴, 12 and 13 ns in ^{26, 27} and ²⁸, respectively.

Based on photoluminescence spectra of the sample zone S2 we calculate emission cross section σ_{em} at the center of the emission band $\lambda_{em} = 680$ nm (See Methods for details). The estimated value reaches $\sigma_{em} = 4.9\cdot10^{-17}$ cm² that is close to the emission cross-section values $4.3\cdot10^{-17}$ cm² and $3.6\cdot10^{-17}$ cm² reported in ²⁶ and ³³, respectively, and it is one order below the value $3.2\cdot10^{-16}$ cm² given in ²⁸. Corresponding absorption cross section at the center of the absorption band $\lambda_{abs} = 569$ nm of zone S2 (See Methods for details) is $\sigma_{abs} = 5.7\cdot10^{-17}$ cm² that matches well with the absorption cross-section values reported in following works: $2.8\cdot10^{-17}$ cm² ²⁶, $(3.1\pm0.8)\cdot10^{-17}$ cm² ³⁵, and $(9.5\pm2.5)\cdot10^{-17}$ cm² ³⁶. Using the obtained absorption cross-section σ_{abs} and corresponding absorption coefficient from Fig. 2a, the concentration of NV⁻ centers is found to be ~ 1.4 ppm ($2.5\cdot10^{17}$ cm⁻³) in the S2 zone. This value lies in the range of the NV⁻ concentrations corresponding to the lasing conditions predicted in ²⁷. Note that in work ²⁶, where lasing was not achieved, the concentration of NV⁻ color centers was $4.5\cdot10^{18}$ cm⁻³, which is an order of magnitude higher than the concentration of NV⁻ centers in the S2 zone of our sample.

Pump-saturation effect of photoluminescence.

To investigate a photoluminescence at high intensity pump rate, we used a picosecond Nd:YAG laser designed in our laboratory that delivers a train of 150-ps pulses delayed by 4.4 ns from each other with possibility of a high contrast selection of a single pulse³⁷. Total energy of the 532-nm pulses train has reached 400 μJ and could be attenuated by set of filters introduced in the optical path. The average light field intensity of pulses train focused into a spot with a diameter of 120 μm (FWHM) reaches about $5 \cdot 10^7 \text{ W/cm}^2$, and the peak intensity of single pulse is $3 \cdot 10^9 \text{ W/cm}^2$, which many orders above the CW lasers intensities. Therefore, this pumping mode delivers a laser-matter interaction regime that drastically differs from the low-power CW laser pump discussed in the previous section.

We have detected experimentally that for both S1 and S2 sample zones the spectral amplitude of NV^0 ZPL at 575 nm grows under pump energy increase (Fig. 3a and b, respectively). In the zone S1 the shape of the luminescence spectrum has characteristic features defined by NV^0 PSB for all considered incident pulse train energies, while NV^- ZPL at 638 nm and its PSB are weakly pronounced. In the zone S2 NV^- PSB defines the luminescence spectrum shape, which has a maximum at ~ 680 nm for low pump energies (Fig. 3b, black curve). The pump energy increase from 0.1 μJ up to 400 μJ leads to the enhancement of the NV^- centers photo-ionization process and corresponding NV^0 concentration growth in the S2 zone. As a result, we observe a saturation of the NV^- contribution and appearance of the NV^0 ZPL and PSB in the range of 575 – 630 nm in the photoluminescence spectrum (Fig. 3b, blue and red curves). The observed pump-saturation effect of NV^- photoluminescence is in a good agreement with the works^{26, 38, 39}, where the role of the NV^- photo-ionization process under pump power increase was investigated.

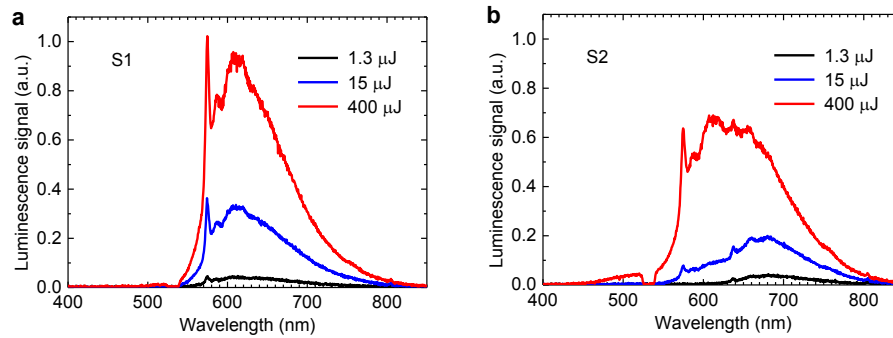


Figure 3 | Pump-saturation effect of photoluminescence. Photoluminescence spectra of **(a)** S1 and **(b)** S2 sample zones under excitation of 532-nm pulsed pump with the pulse train total energy of 1.3 μJ (black curve), 15 μJ (dark gray curve), 400 μJ (light gray curve). The dip in the spectra around the pump wavelength of 532 nm is related to the Thorlabs NF533-17 Notch filter present in the scheme. The spectra were recorded in transmission configuration; the pump laser and the recording spectrometer were located on opposite sides of the sample.

Stimulated emission from NV^- centers in diamond.

We employed a direct pump-probe method for stimulated emission registration from the S1 and S2 zones of the diamond sample (Fig. 4). A 675-nm Thorlabs HL6750MG CW laser diode with 100-mW power was used to probe the sample. In the first series of experiments, the sample was placed perpendicularly to the probe beam at a 150-mm distance from the laser diode. An 11-mm lens creates a 50- μm (FWHM) probe beam waist at the sample surface (Fig. 4, inset 1). A vertical translator with a micrometer resolution provided an opportunity to switch between the studied sample zones S1 and S2. In this case, to pump the sample in a single-pulse regime, we cut the central laser pulse from a pulse train of 150-ps pulses³⁷. The energy of the 532-nm single pulse was controlled by attenuating filters in the range from 0.6 to 15 μJ . The waist diameter of the pump beam focused by a 150-mm lens on the sample surface was about 120 μm (FWHM). An interference filter for 675 – 680 nm was placed at the entrance of a collimator Thorlabs F220FC-1064, which collected the laser diode radiation passed through the sample into the measuring optical fiber. To minimize the influence of spontaneous luminescence, the collecting collimator is located at a distance of about 200 mm from the sample. The stimulated emission was detected by a LeCroy WaveMaster 808Zi-A oscilloscope

with a LeCroy OE555 optoelectronic converter with 4.5 GHz sample rate, which allows to study in real time the dynamics probe amplification in the sample under picosecond laser pump.

In the second series of experiments a cylindrical lens was employed to create an elliptical pump beam profile illuminating the whole zone S2 with surface area of about 4×0.25 mm. Since the pump beam area was increased significantly, we apply the full train of 15 picosecond pulses, instead of a single pump pulse. The sample was placed at the Brewster's angle to the probe beam, so that the probe beam was going along the diamond parallel to sample side surfaces (Fig. 4, inset 2). Note, that conventional Q-switched nanosecond Nd:YAG lasers usually have a stochastic structure of resonator light field time profile, which leads to significant pulse-to-pulse intensity variations with cavity round-trip period features. Such pump pulses cannot allow a controlled uniform pumping of the sample. In opposite, the train of active mode-locked picosecond laser pulses employed in our experiments has high temporal regularity and shot-to-shot repeatability³⁷.

The kinetics of the probe laser diode signal transmitted through the sample zones S1 and S2 are shown in Fig. 5a and b, respectively. The signal was normalized to the level of the unperturbed laser diode signal transmitted through the sample in the absence of a pump pulse. The 532-nm picosecond pump pulse arrives at moment in time $t = 0$, and leads to a disturbance of the detected 675-nm signal.

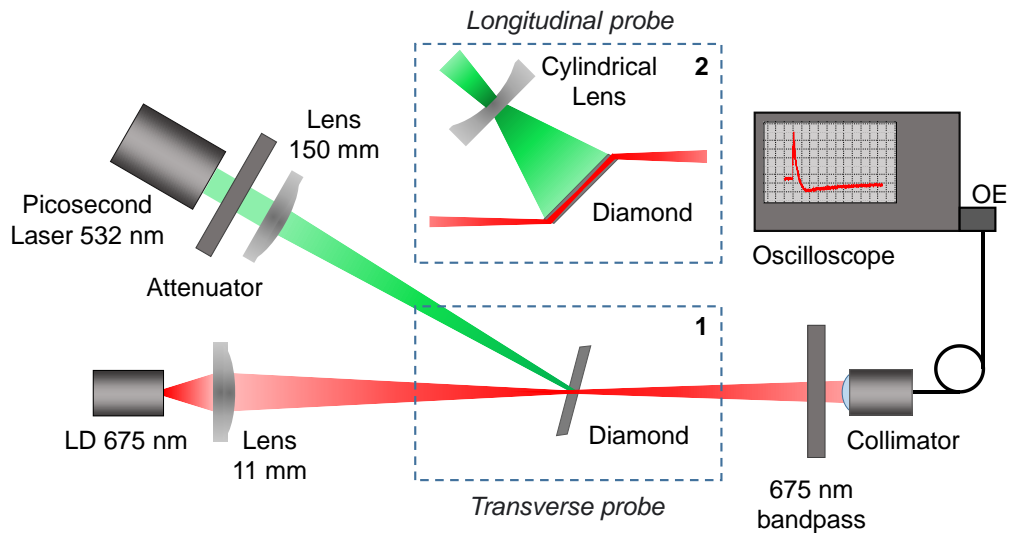


Figure 4 | Experimental setup. Scheme of a pump-probe experiment for registration of stimulated emission from the diamond sample. We employed transverse probe configuration in which the sample was placed perpendicularly to the probe beam (inset 1) and longitudinal probe configuration in which probe beam was going along the diamond parallel to sample side surfaces (inset 2).

In the S1 zone, characterized by the presence of the NV^0 centers, the appearance of a pump pulse leads to an attenuation of the probe signal at all the considered pump energies (Fig. 5a). The leading edge of the transient response has a duration of less than 100 ps, which corresponds to the profile of the pump pulse. The relaxation process of the pump-induced absorption is essentially nonlinear and its characteristic time depends on the energy of the pump pulse. For pump energy below $1 \mu J$, the relaxation time is about 20 ns; for higher pump energies, the complete relaxation was not reached at times up to $10 \mu s$. In this case, the relaxation process cannot be decomposed into fast and slow components and looks rather like a multi-particle process with a smooth change in the relaxation rate.

In the S2 zone, characterized by the predominance of the NV^- centers, we registered the pump induced amplification of the probe signal (Fig. 5b). For pump energies below $7 \mu J$, the relaxation process of the pump-induced amplification has a characteristic time about 10 ns (Fig. 5b, black, blue and green curves), which is close to the lifetime of the NV^- excited state, since the probe beam has a relatively weak intensity. The maximum registered gain is about 1.05 at a pump

pulse energy of $6.6 \mu\text{J}$. Taking the sample depth as 0.25 mm and stimulated emission cross-section $\sigma_{\text{em}} = 4.9 \cdot 10^{-17} \text{ cm}^2$ (see the first section), the concentration of the pumped NV^- centers reaches $0.4 \cdot 10^{17} \text{ cm}^{-3}$ that is about 16% from the total concentration of the NV^- centers in the S2 zone.

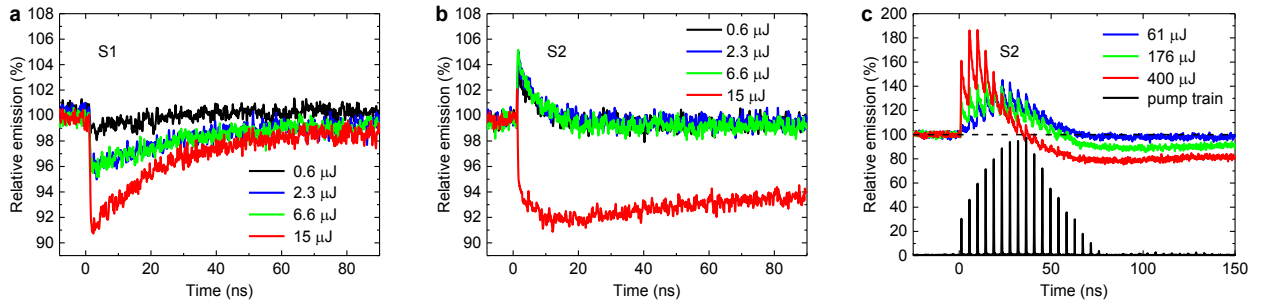


Figure 5 | Stimulated emission from diamond sample. Kinetics of the laser diode signal in a wavelength range from 675 nm to 680 nm transmitted through the sample zones S1 **(a)** and S2 **(b)** pumped by a single 150-ps 532-nm pulse at various energies: $0.6 \mu\text{J}$ (black curve), $2.3 \mu\text{J}$ (blue curve), $6.6 \mu\text{J}$ (green curve), $15 \mu\text{J}$ (red curve) in case of transverse probe configuration (Fig. 4, inset 1). **(c)** Kinetics of the 675-nm laser diode signal transmitted through the sample zone S2 pumped by a train of 150-ps 532-nm laser pulses at various energies: $61 \mu\text{J}$ (blue curve), $176 \mu\text{J}$ (green curve), and $400 \mu\text{J}$ (red curve) in case of longitudinal probe configuration (Fig. 4, inset 2). Corresponding train of pump pulses with normalized amplitudes is plotted as a black curve. The front weak pulses of the train were dumped by a pulse selector.

At a pump energy of $15 \mu\text{J}$, the ionization process of the NV^- centers and corresponding growth of the NV^0 concentration leads to a transition from the probe signal amplification to the probe signal absorption that occurs on a 1.5-ns time scale (Fig. 5b, red curve). The dynamics of the induced-absorption relaxation process is identical to the dynamics in the S1 zone. Thus, the process of induced absorption correlates with the presence of NV^0 centers in the studied sample, regardless of whether they were present initially or were formed as a result of pulse-induced ionization of NV^- centers.

From the obtained kinetics of the probe signal, it is clear that there is a pump rate threshold, an exceeding of which leads to saturation of probe gain and further switch to an attenuation of the probe signal. Due to the demonstrated pump-saturation behavior of the probe gain, we consider a side pump configuration along the sample allowing us to reach a higher gain level. A

cylindrical lens was employed to create an elliptical pump beam profile illuminating the crystal zone S2 with surface area of about 4×0.25 mm. Since the pump beam area was increased significantly, we apply the full train of 15 picosecond pulses, instead of a single pump pulse. The sample was placed at the Brewster's angle to the probe beam, so that the probe beam was going along the diamond parallel to sample side surfaces (Fig. 4, inset 2). The S1 zone of the sample was not considered in this series of experiments, due to no stimulated emission was observed in this zone.

Recorded kinetics of the probe signal transmitted through the sample shown in Fig. 5c for various energies of a multi-pulse pump. At low pump energy of $61 \mu\text{J}$, the probe amplification profile repeats the intensity profile of the pump pulse train (Fig. 5c, blue curve). At higher pump energy of $176 \mu\text{J}$, weak probe absorption appears at the end of the pump train (Fig. 5c, green curve). A saturation of probe amplification followed by NV^- -ionization induced absorption occurs at sufficiently high pump energy of $400 \mu\text{J}$ (Fig. 5c red curve). Further increase of the pump energy will lead to an over-threshold pumping regime that does not provide optimal lasing conditions. The maximum achieved gain is 1.8 (gain coefficient 1.5 cm^{-1}), which is quite sufficient for stable lasing conditions. The corresponding concentration of excited NV^- centers reaches $0.3 \cdot 10^{17} \text{ cm}^{-3}$, that is about 12% from the total concentration of the NV^- centers in the S2 zone.

Lasing on NV^- centers in diamond

Herein we report the scheme of the resonator, used for demonstration of the lasing on NV^- centers in diamond, and the characterization of the lasing pulses. The resonator consists of two identical flat mirrors with reflection coefficient 95% in the range of wavelengths from 700 to 750 nm. The diamond sample was aligned at the Brewster's angle in resonator that provides a lasing direction along the sample. In order to compensate the beam divergence and to increase

the resonator stability, a BK7 spherical lens with focal length of 15 mm was introduced in the resonator at the Brewster's angle to the beam axis (Fig. 6a). The cavity length was chosen to provide a symmetrical mode on one of the mirrors (Fig. 6d). We were operating with the sample zone S2, in which the stimulated emission has been obtained. A full train of 150-ps 532-nm laser pulses was used to pump the sample. As in the previous section, the cylindrical lens was employed for side illumination of the whole S2 zone of the sample.

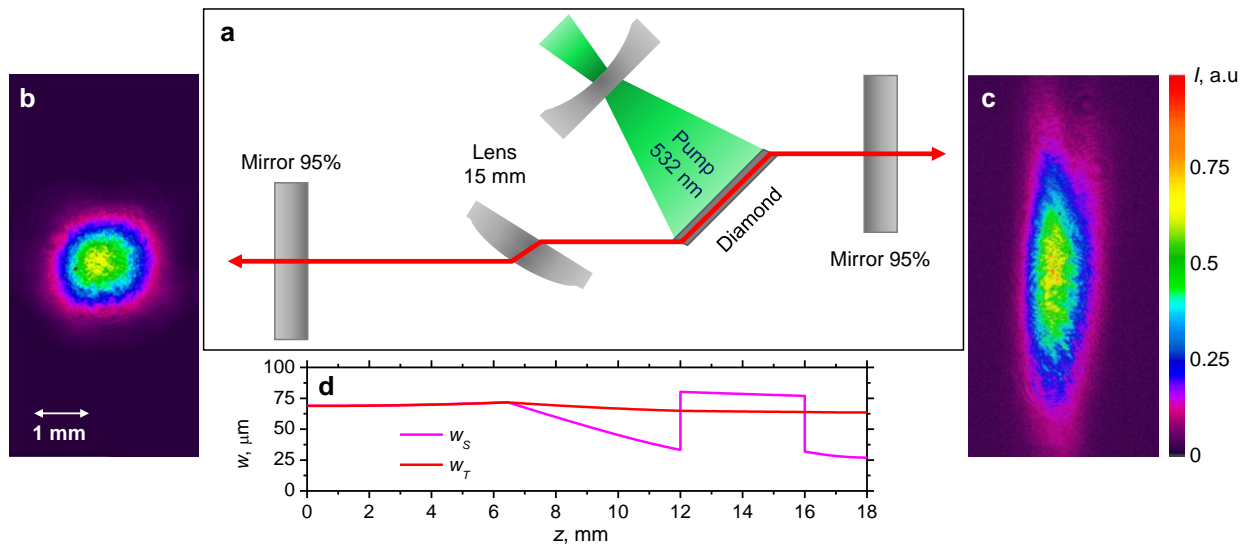


Figure 6 | NV⁻ Diamond Laser. (a) Resonator scheme of the NV⁻ color centers diamond laser. (b), (c) Beam profiles at a distance of 200 mm from the resonator mirrors. (d) Calculated transverse mode radius w_T and sagittal mode radius w_S along the resonator (intensity e^{-2} level).

A laser generation at NV⁻ color centers in diamond was obtained under pump energies of ps-pulse train above 35 μJ . The maximal energy of the achieved laser pulse reaches 10 nJ (5 nJ at each output coupler) under 260- μJ pump. Spatial profiles of lasing mode were recorded at 200-mm distances from each output coupler by the Ophir SP620U CCD camera and are shown in Fig. 6b and c. The polarization measurements show that the laser beam is linear polarized according to the Brewster's angle of diamond sample.

Temporal profiles of the lasing pulse at various pump energies are given in Fig. 7a. The minimal lasing pulse duration of about 1 ns (FWHM) has been achieved for pump energies from 73 μJ to 140 μJ (Fig. 7a violet and blue curves). The active media inversion population changes

dramatically on the time scale of a delay between the neighboring pulses in the pump train because the lifetime of the NV^- excited state (about 10 ns) is comparable to the 4.4-ns delay between pump pulses in the train. In this case the minimal laser pulse duration can be achieved if the laser generation develops in resonator after the arrival of the second pulse from the pump pulse train. At high pump energies (260 μJ and 400 μJ), the lasing development occurs between the first and the second pump pulses of the train and corresponding lasing pulse time profile consists of several peaks (Fig. 7a red and black curves).

The laser pulse spectrum has a maximum at 720 nm (Fig. 7b) and a width of 20 nm (FWHM). Lasing process starts from noise in the entire gain band and the pulse rise time in the cavity (~ 5 ns, 20 – 30 roundtrips) is sufficiently for lasing spectrum narrowing by about an order in comparison with luminescence spectrum width (Fig. 7b).

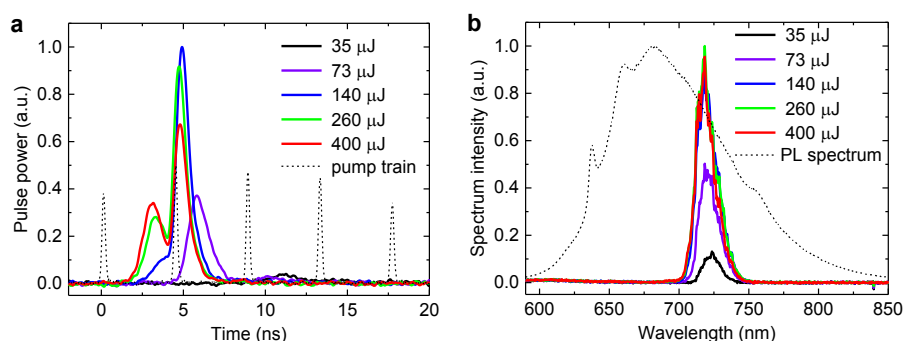


Figure 7 | Lasing pulse characteristics. Time profiles of lasing pulses (a) and lasing spectra (b) at various pump pulse train energies: 35 μJ (black curve), 73 μJ (violet curve), 140 μJ (blue curve), 260 μJ (green curve) and 400 μJ (red curve). Black dashed curves: train of pump pulses with normalized amplitudes (a) and photoluminescence spectrum of S2 zones of diamond sample under continuous excitation at 532 nm (b).

Conclusion

Comparative spectroscopic studies have proven the possibility of lasing in diamond samples containing NV^- color centers with densities about 10^{17} cm^{-3} . The presence of NV^0 centers, regardless of whether they were initially contained in the sample or were formed during the NV^- ionization process under a high-intensity laser pumping, leads to a decrease of the

stimulated emission and a transition to the probe absorption regime. We conclude that for 532-nm pump wavelength there is an optimal pumping rate at which the highest gain in the NV⁻ diamond is achieved. The maximum reached gain is 1.8 (gain coefficient 1.5 cm⁻¹) when the sample zone containing NV⁻ centers was pumped by a train of picosecond pulses. Stable lasing at a wavelength of 720 nm was achieved in diamond sample under optimal pumping conditions. Compelling experimental evidence on lasing were observed: 10-nJ pulse energy, a near diffraction limited laser beam, linear polarization, nanosecond pulse temporal profile, and lasing spectrum narrowing by about an order in comparison with luminescence spectrum width.

The achieved lasing at NV⁻ color centers in diamond will lead to an enhancement of a broad laser system development based on the NV⁻ diamond active media. A unique combination of properties such as thermal conductivity, low thermal expansion, and mechanical strength makes diamond crystals an excellent candidate for high-power CW and ultrashort lasers.

Methods

Diamond sample preparation.

A diamond sample is a 4×3×0.25 mm plate cut from HPHT diamond subjected to a radiation treatment by electrons accelerated to 3 MeV with a dose of about 1·10¹⁸ e⁻/cm² and subsequent annealing in vacuum at a temperature of 800 °C for 24 hours. Two lateral sides of the sample were polished at 22.5-degree angle to enable studies of the probe amplification incident on the sample at the Brewster's angle (67.5 degrees).

The diamond sample has two growth zones with significantly different concentrations of nitrogen, which is incorporated into the diamond lattice during HPHT synthesis. Most of the diamond sample has a nitrogen concentration of less than 1 ppm (zone S1), while the narrow colored area at the edge of the sample has a nitrogen concentration that is about 2 orders of

magnitude higher (zone S2). NV complexes are formed in the crystal after irradiation with 3 MeV electrons and annealing in vacuum at 800 °C. In the S1 sample zone with a low nitrogen content, a significant fraction (about a half) of nitrogen atoms have formed impurity-defect complexes (NV centers) with vacancies in a neutral charge state. In the zone of the diamond sample with an increased concentration of nitrogen S2 (colored region), the main part of nitrogen remained in the form of single substitutional atoms, which are a donor impurity. In S2 zone, excess electrons from some of the substitutional nitrogen atoms were captured by NV centers. Thus, in the colored region of sample S2, NV centers in the negative charge state were formed, while keeping a negligible fraction of original NV centers in the neutral charge state.

Emission and absorption cross-sections of the sample

For S2 zone of the sample, we estimate emission and absorption cross-sections based on the spectroscopic sample characteristics (Fig. 2). Here we take the fluorescence quantum efficiency being close to 1. The emission cross section was calculated at the center of the emission band $\lambda_{em} = 680$ nm assuming a Gaussian emission line shape in the frequency domain ⁴⁰⁻⁴⁴:

$$\sigma_{em} = \frac{\lambda_{em}}{4\pi n^2 \tau_{21} \Delta\nu_{em}} \left(\frac{\ln 2}{\pi} \right)^{\frac{1}{2}}, \quad (1)$$

where emission band is fitted by a Gaussian line shape with a width FWHM $\Delta\nu = 66$ THz that corresponds to $\Delta\omega = 0.27$ eV ($2.2 \cdot 10^3$ cm⁻¹) and $\omega_0 = 1.81$ eV ($1.46 \cdot 10^4$ cm⁻¹). The estimated emission cross-section value reaches $\sigma_{em} = 4.9 \cdot 10^{-17}$ cm². We estimate absorption cross section at the center of the absorption band $\lambda_{abs} = 569$ nm assuming also a Gaussian emission line shape in the frequency domain ⁴⁰⁻⁴⁴:

$$\sigma_{abs} = \frac{g_2}{g_1} \frac{\lambda_{abs}}{4\pi n^2 \tau_{21} \Delta\nu_{abs}} \left(\frac{\ln 2}{\pi} \right)^{\frac{1}{2}}, \quad (2)$$

where $g_1 = 1$ and $g_2 = 2$ are degeneracies of ground and excited states, respectively, absorption band is fitted by a Gaussian line shape with a width FWHM $\Delta\nu = 78$ THz, that corresponds to

$\Delta\omega = 0.33 \text{ eV}$ ($2.7 \cdot 10^3 \text{ cm}^{-1}$) and $\omega_0 = 2.16 \text{ eV}$ ($1.7 \cdot 10^4 \text{ cm}^{-1}$). The estimated absorption cross-section value reaches $\sigma_{abs} = 5.7 \cdot 10^{-17} \text{ cm}^2$.

Data availability.

The data that support the findings of this study are available from the corresponding author on request.

References

1. Zaitsev, A.M. *Optical Properties of Diamond* (Springer-Verlag, Berlin Heidelberg, 2001).
2. Mironov, V., Martynovich, E. & Grigorov, V.A. Laser materials on the base of a diamond in *Physics and technology of diamond materials* 96-111 (Polaron, Moscow, 1994).
3. Rand, S.C. & DeShazer, L.G. *Laser action of H3 color center in diamond* (Springer-Verlag, 1985).
4. Pereira, E. & Santos, L. Dynamics of S3 luminescence in diamond. *Journal of Luminescence* **45**, 454-457 (1990).
5. Ditalia Tchernij, S. et al. Fluorine-based color centers in diamond. *Scientific Reports* **10**, 1-7 (2020).
6. Walker, J. Optical absorption and luminescence in diamond. *Reports on Progress in Physics* **42**, 1605-1659 (1979).
7. Rand, S.C. & DeShazer, L.G. Visible color-center laser in diamond. *Optics Letters* **10**, 481 (1985).
8. Mildren, R.P. & Sabella, A. Highly efficient diamond Raman laser. *Optics Letters* **34**, 2811 (2009).
9. Aharonovich, I., Englund, D. & Toth, M. Solid-state single-photon emitters. *Nature Photonics* **10**, 631-641 (2016).
10. Bogdanov, S.I. et al. Ultrafast quantum photonics enabled by coupling plasmonic nanocavities to strongly radiative antennas. *Optica* **7**, 463 (2020).
11. Pezzagna, S., Rogalla, D., Wildanger, D., Meijer, J. & Zaitsev, A. Creation and nature of optical centres in diamond for single-photon emission-overview and critical remarks. *New Journal of Physics* **13**, 35024 (2011).
12. OIDA. OIDA Quantum Photonics Roadmap: Every Photon Counts (Optical Society of America, 2020).
13. Wu, Y., Wang, Y., Qin, X., Rong, X. & Du, J. A programmable two-qubit solid-state quantum processor under ambient conditions. *npj Quantum Information* **5**, 1-5 (2019).
14. Bradley, C.E. et al. A Ten-Qubit Solid-State Spin Register with Quantum Memory up to One Minute. *Physical Review X* **9**, 031045 (2019).
15. Pinto, D. et al. Readout and control of an endofullerene electronic spin. *Nature Communications* **11**, 1-6 (2020).
16. McCullian, B.A. et al. Broadband multi-magnon relaxometry using a quantum spin sensor for high frequency ferromagnetic dynamics sensing. *Nature Communications* **11**, 1-8 (2020).
17. Irber, D.M. et al. Robust all-optical single-shot readout of nitrogen-vacancy centers in diamond. *Nature Communications* **12**, 532 (2021).

18. Lühmann, T., John, R., Wunderlich, R., Meijer, J. & Pezzagna, S. Coulomb-driven single defect engineering for scalable qubits and spin sensors in diamond. *Nature Communications* **10**, 1-9 (2019).
19. Orwa, J.O. et al. Fabrication of single optical centres in diamonds: a review. *Journal of Luminescence* **130**, 1646-1654 (2010).
20. Gruber, A. et al. Scanning confocal optical microscopy and magnetic resonance on single defect centers. *Science* **276**, 2012-2014 (1997).
21. Giovannetti, V., Lloyd, S. & MacCone, L. Advances in quantum metrology. *Nature Photonics* **5**, 222-229 (2011).
22. Kuwahata, A. et al. Magnetometer with nitrogen-vacancy center in a bulk diamond for detecting magnetic nanoparticles in biomedical applications. *Scientific Reports* **10**, 1-9 (2020).
23. Ariyaratne, A., Bluvstein, D., Myers, B.A. & Jayich, A.C.B. Nanoscale electrical conductivity imaging using a nitrogen-vacancy center in diamond. *Nature Communications* **9**, 1-7 (2018).
24. Liu, G.Q., Feng, X., Wang, N., Li, Q. & Liu, R.B. Coherent quantum control of nitrogen-vacancy center spins near 1000 kelvin. *Nature Communications* **10**, 1-8 (2019).
25. Jensen, K. et al. Cavity-enhanced room-temperature magnetometry using absorption by nitrogen-vacancy centers in diamond. *Physical Review Letters* **112**, 160802 (2014).
26. Subedi, S.D. et al. Laser spectroscopic characterization of negatively charged nitrogen-vacancy (NV⁻) centers in diamond. *Optical Materials Express* **9**, 2076 (2019).
27. Jeske, J. et al. Stimulated emission from nitrogen-vacancy centres in diamond. *Nature Communications* **8**, 370 (2017).
28. Vins, V.G. & Pstryakov, E.V. Color centers in diamond crystals: Their potential use in tunable and femtosecond lasers. *Diamond and Related Materials* **15**, 569-571 (2006).
29. Rubinas, R. et al. Spin properties of NV centers in high-pressure, high-temperature grown diamond. *Journal of Physics Communications* **2**, 115003 (2018).
30. Rubinas, O.R. et al. Optimization of the coherence properties of diamond samples with an intermediate concentration of NV centers. *arXiv* (2020).
31. Yakubovskii, K. & Adriaenssens, G.J. Optical transitions at the substitutional nitrogen centre in diamond. *Journal of Physics Condensed Matter* **12**, L77 (2000).
32. Goss, J.P., Briddon, P.R., Jones, R. & Sque, S. Donor and acceptor states in diamond. *Diamond and Related Materials* **13**, 684-690 (2004).
33. Fraczek, E. et al. Laser spectroscopy of NV⁻ and NV⁰ colour centres in synthetic diamond. *Optical Materials Express* **7**, 2571 (2017).
34. Batalov, A. et al. Temporal coherence of photons emitted by single nitrogen-vacancy defect centers in diamond using optical Rabi-oscillations. *Physical Review Letters* **100**, 077401 (2008).
35. Wee, T.L. et al. Two-photon excited fluorescence of nitrogen-vacancy centers in proton-irradiated type Ib diamond. *Journal of Physical Chemistry A* **111**, 9379-9386 (2007).
36. Chapman, R. & Plakhotnik, T. Quantitative luminescence microscopy on Nitrogen-Vacancy Centres in diamond: Saturation effects under pulsed excitation. *Chemical Physics Letters* **507**, 190-194 (2011).
37. Savvin, A., Sirotkin, A., Mitrokhin, V. & Dormidonov, A. Picosecond Diode Pumped Nd:YAG Laser for Initiation of Localized Energetic Processes in Non-laboratory Applications. *Proceedings - 2020 7th International Congress on Energy Fluxes and Radiation Effects, EFRE 2020*, 1048-1052 (2020).

38. Aslam, N., Waldherr, G., Neumann, P., Jelezko, F. & Wrachtrup, J. Photo-induced ionization dynamics of the nitrogen vacancy defect in diamond investigated by single-shot charge state detection. *New Journal of Physics* **15**, 013064 (2013).
39. Hacquebard, L. & Childress, L. Charge-state dynamics during excitation and depletion of the nitrogen-vacancy center in diamond. *Physical Review A* **97**, 063408 (2018).
40. Davis, C.C. Lasers and electro-optics, second edition (Cambridge University Press, 2013).
41. Fowler, W.B. & Dexter, D.L. Relation between absorption and emission probabilities in luminescent centers in ionic solids. *Physical Review* **128**, 2154-2165 (1962).
42. Koechner, W. Solid-State Laser Engineering (Springer, New York, 2006).
43. Subedi, S.D. et al. Laser spectroscopy of highly doped NV⁻ centers in diamond. *Proc.SPIE* **10511** (2018).
44. Mooney, J. & Kambhampati, P. Correction to “Get the Basics Right: Jacobian Conversion of Wavelength and Energy Scales for Quantitative Analysis of Emission Spectra”. *The Journal of Physical Chemistry Letters* **5**, 3497 (2014).

Acknowledgements

EL and DG acknowledge the Ministry of Education and Science of Russian Federation for funding the research (the state order, project No 0721-2020-0048).

Author contributions

AS, AD and EL conceived and planned the experiments. AY, EL and DG carried out the spectroscopic characterization of the diamond sample. AS, AD, VM and SP carried out the main experiments. AY and VV contributed to diamond sample preparation. AD, EL, ES, and AS contributed to the interpretation of the results. AD and ES took the lead in writing the manuscript. All authors provided critical feedback and helped shape the research, analysis and manuscript.

Competing interests

The authors declare no competing interests.

Figures Legends

Figure 1 | The diamond sample. Photography of the diamond sample that has two growth zones with significantly different ratios of NV^0 concentration to NV^- concentration. Zone S1 mainly contains neutral NV^0 centers and NV^- concentration dominates in zone S2.

Figure 2 | Spectroscopic characterization of the diamond sample. (a) Absorption spectrum of S1 (gray curve) and S2 (black curve) zones of diamond sample. The spectra were recorded at room temperature. Normalized photoluminescence spectra of S1 **(b)** and S2 **(c)** zones under continuous excitation at various wavelengths: 532 nm (green curve), 450 nm (blue curve), and 400 nm (violet curve). For each pump wavelength the spectra collected from both zones were normalized on the S1-zone spectral amplitude at 575 nm that corresponds to the NV^0 zero-phonon line. The photoluminescence spectra were collected from the sample excitation surface, i.e. the pump lasers and the recording spectrometer were located on the same side of the sample.

Figure 3 | Pump-saturation effect of photoluminescence. Photoluminescence spectra of **(a)** S1 and **(b)** S2 sample zones under excitation of 532-nm pulsed pump with the pulse train total energy of 1.3 μJ (black curve), 15 μJ (dark gray curve), 400 μJ (light gray curve). The dip in the spectra around the pump wavelength of 532 nm is related to the Thorlabs NF533-17 Notch filter present in the scheme. The spectra were recorded in transmission configuration; the pump laser and the recording spectrometer were located on opposite sides of the sample.

Figure 4 | Experimental setup. Scheme of a pump-probe experiment for registration of stimulated emission from the diamond sample. We employed transverse probe configuration in which the sample was placed perpendicularly to the probe beam (inset 1) and longitudinal

probe configuration in which probe beam was going along the diamond parallel to sample side surfaces (inset 2).

Figure 5 | Stimulated emission from diamond sample. Kinetics of the laser diode signal in a wavelength range from 675 nm to 680 nm transmitted through the sample zones S1 **(a)** and S2 **(b)** pumped by a single 150-ps 532-nm pulse at various energies: 0.6 μJ (black curve), 2.3 μJ (blue curve), 6.6 μJ (green curve), 15 μJ (red curve) in case of transverse probe configuration (Fig. 4, inset 1). **(c)** Kinetics of the 675-nm laser diode signal transmitted through the sample zone S2 pumped by a train of 150-ps 532-nm laser pulses at various energies: 61 μJ (blue curve), 176 μJ (green curve), and 400 μJ (red curve) in case of longitudinal probe configuration (Fig. 4, inset 2). Corresponding train of pump pulses with normalized amplitudes is plotted as a black curve. The front weak pulses of the train were dumped by a pulse selector.

Figure 6 | NV⁻ Diamond Laser. **(a)** Resonator scheme of the NV⁻ color centers diamond laser. **(b), (c)** Beam profiles at a distance of 200 mm from the resonator mirrors. **(d)** Calculated transverse mode radius w_T and sagittal mode radius w_S along the resonator (intensity e^{-2} level).

Figure 7 | Lasing pulse characteristics. Time profiles of lasing pulses **(a)** and lasing spectra **(b)** at various pump pulse train energies: 35 μJ (black curve), 73 μJ (violet curve), 140 μJ (blue curve), 260 μJ (green curve) and 400 μJ (red curve). Black dashed curves: train of pump pulses with normalized amplitudes **(a)** and photoluminescence spectra of S2 zones of diamond sample under continuous excitation at 532 nm **(b)**.